

Search of MeV–GeV counterparts of TeV sources with AGILE in pointing mode[★]

A. Rappoldi¹, F. Lucarelli^{2,3}, C. Pittori^{2,3}, F. Longo^{4,5}, P. W. Cattaneo¹, F. Verrecchia^{2,3}, M. Tavani^{6,7}, A. Bulgarelli⁸, A. W. Chen⁹, S. Colafrancesco⁹, I. Donnarumma⁶, A. Giuliani¹⁰, A. Morselli¹¹, S. Sabatini⁶, and S. Vercellone¹²

¹ INFN–Pavia, via Bassi 6, 27100 Pavia, Italy
e-mail: andrea.rappoldi@pv.infn.it

² ASI Science Data Center, via del Politecnico snc, 00133 Roma, Italy

³ INAF–Osservatorio Astronomico di Roma, via di Frascati 33, 00040 Monteporzio Catone, Roma, Italy

⁴ INAF–Osservatorio Astronomico di Trieste, via G.B. Tiepolo 11, 34143 Trieste, Italy

⁵ INFN–Trieste, Padriciano 99, 34012 Trieste, Italy

⁶ INAF-IAPS Roma, via Fosso del Cavaliere 100, 00133 Roma, Italy

⁷ Dip. di Fisica, Università “Tor Vergata”, via della Ricerca Scientifica 1, 00133 Roma, Italy

⁸ INAF–IASF Bologna, via Gobetti 101, 40129 Bologna, Italy

⁹ School of Physics, University of the Witwatersrand, Johannesburg Wits 2050, South Africa

¹⁰ INAF–IASF Milano, via E. Bassini 15, 20133 Milano, Italy

¹¹ INFN–Roma Tor Vergata, via della Ricerca Scientifica 1, 00133 Roma, Italy

¹² INAF–IASF Palermo, via Ugo La Malfa 153, 90146 Palermo, Italy

Received 9 June 2015 / Accepted 2 December 2015

ABSTRACT

Context. Known TeV sources detected by major Čerenkov telescopes are investigated to identify possible MeV–GeV γ -ray counterparts.

Aims. A systematic study of the known sources in the web-based TeVCat catalog has been performed to search for possible γ -ray counterparts on the AGILE data collected during the first period of operations in observing pointing mode.

Methods. For each TeV source, a search for a possible γ -ray counterpart that is based on a multi-source maximum likelihood algorithm is performed on the AGILE data taken with the GRID instrument from July 2007 to October 2009.

Results. In the case of high-significance detection, the average γ -ray flux is estimated. For cases of low-significance detection the 95% confidence level (CL) flux upper limit is given. 52 TeV sources out of 152 (corresponding to $\sim 34\%$ of the analysed sample) show a significant excess in the AGILE data covering the pointing observation period.

Conclusions. This analysis found 26 new AGILE sources with respect to the AGILE reference catalogs, 15 of which are galactic, 7 are extragalactic and 4 are unidentified. Detailed tables with all available information on the analysed sources are presented.

Key words. catalogs – gamma rays: general

1. Introduction

In the last years, the number of identified TeV sources has increased up to more than 100, thanks to the observations made by the new generation of ground-based Čerenkov telescopes HESS (Hinton 2004), MAGIC (Ferenc 2005) and VERITAS (Holder et al. 2006). These sources mainly belong to five classes: active galactic nuclei (AGN), supernova remnants (SNR), pulsar wind nebulae (PWN), X-rays binary systems (XRB), and pulsars (PSR). More than 80 TeV sources are galactic and a significant fraction of them ($\geq 20\%$) do not show any evident counterpart and remain unidentified (UNID).

Multi-wavelength deep observations of the regions near the TeV sources are needed to identify the possible counterparts of the UNID, as well as to understand the emission mechanisms of the TeV γ -rays.

Following previous studies on the positional and spectral connection of GeV to TeV γ -ray sources performed on EGRET and *Fermi*-LAT data (Funk et al. 2008, 2013; Abdo et al. 2009; Acero et al. 2013), this paper reports the results of the search for γ -ray emission from known and unidentified TeV sources, using the data collected by AGILE in pointing mode in the energy range above 100 MeV.

This search is particularly relevant, as demonstrated by previous studies, because the two adjacent energy ranges probe different regions of the source spectra. Preliminary results have been previously presented (Rappoldi et al. 2011; Longo et al. 2011).

2. The TeV source catalog

The analysis described in this paper has been applied to a reference sample of TeV sources extracted from the online TeVCat catalog¹. This online catalog is continuously updated with new

[★] An interactive online version of the considered source list including all the analysis results is also available at the website <http://www.asdc.asi.it/agiletevcat/>

¹ <http://tevcats.uchicago.edu/> (Wakely, S., and Horan, D.).

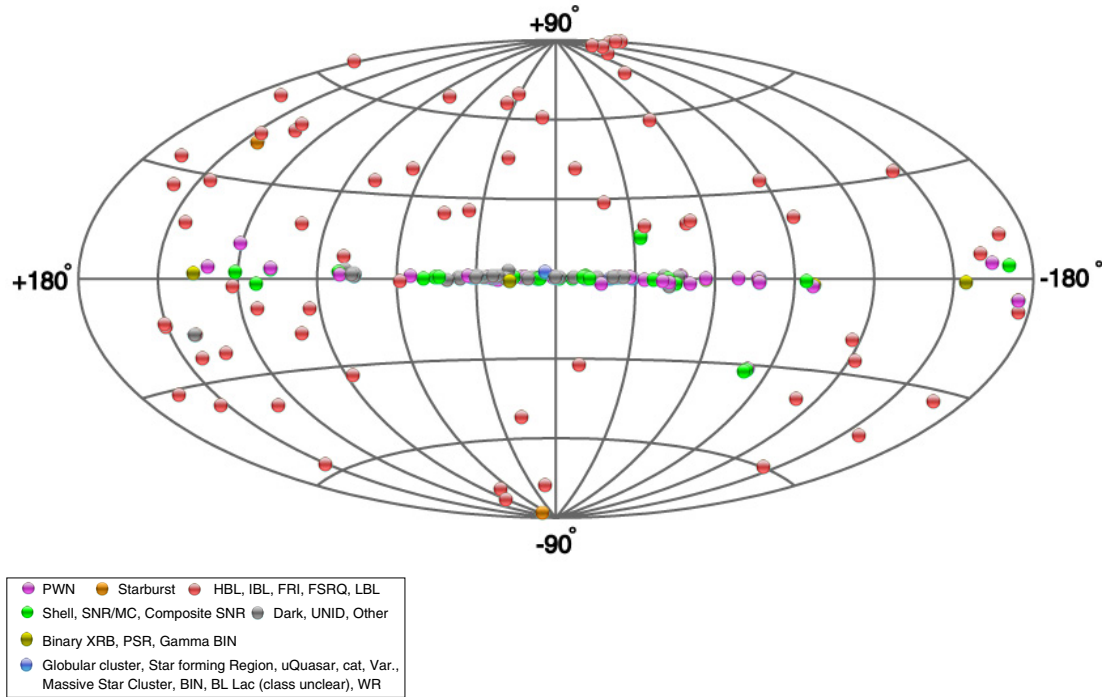


Fig. 1. Aitoff projection in Galactic coordinates of the TeV source positions, as extracted from the online TeVCat (“default catalog” and “newly announced” samples, June 2015; Wakely & Horan).

sources detected by TeV experiments, and for each source it provides many parameters such as coordinates, source type, flux, and estimated distance (when available).

At the time of writing (June 2015), the TeVCat catalog contains a total of 183 TeV sources: 129 of those are flagged as “default catalog” and have been published on refereed journals, 32 are flagged as “newly announced” (see also Fig. 1), ten are flagged as “other sources” and 12 are flagged as “sources candidates”. The analysis described here was performed on a subset of 152 TeV sources, both galactic and extragalactic, consisting of 120 sources of the “default catalog”, plus 32 “newly announced” sources. The following criteria were adopted to define the input sample. Three “extended regions”, which already include a compact TeV source, were excluded: the Galactic Centre Ridge (including HESS J1745-290 and SNR G 0.9+0.1), Boomerang PWN (including SNR G 106.3+2.7) and Milagro Diffuse (including MGRO J2019+37). The TeV sources SN 1006 SW and NE, HESS J1018-589 A and B as well as HESS J1800-240 A and B, were considered as single candidate γ -ray sources located, respectively, at the centre of the SNR 1006 shell, and at the centroid positions of HESS J1018-589 and HESS J1800-240. The two TeV sources ARGO J2031+4157 and MGRO J2031+41 were not included since they are both associated with TeV J2032+415 in the TeVCat. Moreover, the detection of the pulsed emission at TeV energies from the Crab and Vela Pulsar has not been considered in the sample since the timing analysis of pulsars is out of the scope of this paper.

Each sky position and extension of the TeV sources in the selected TeVCat sample has been carefully reviewed using published data. A new interactive web page of the catalog of TeV sources, including this coordinate revision and giving public access to light curves and spectra, is now available at the ASI Science Data Center (ASDC; Carosi et al. in press 2015)².

When available, the best-fit position of the TeV excess has been used as starting input position for the AGILE data analysis. Otherwise, the position of the optical/radio known counterpart has been used. The error region on each TeV source position has been calculated by quadratically summing the statistical uncertainties on the position coordinates that were obtained from the 2D-Gaussian fit of the TeV excess, and the systematic uncertainties on the instrument pointing (when available in the literature).

3. The AGILE satellite

AGILE (Tavani et al. 2009) is an Italian Space Agency (ASI) small scientific mission for high-energy astrophysics launched on April 23, 2007 from the Indian base of Sriharikota in an equatorial orbit optimised for low particle background, with a very small inclination angle ($\sim 2.5^\circ$) and initial altitude of about 550 km.

The analysis has been performed using the data collected by the main AGILE instrument, the Gamma-Ray Imaging Detector (GRID). The AGILE-GRID is sensitive in the energy range 30 MeV–50 GeV and consists of a silicon-tungsten tracker, a caesium iodide mini-calorimeter, and an anticoincidence system made up of segmented plastic scintillators. The use of the silicon strip technology allows to have good performance for the γ -ray GRID imager, approximately a small cube of ~ 60 cm size, which achieves an effective area of approximately 500 cm² at several hundreds MeV, an angular resolution (at 68% containment radius) of about 4.3° at 100 MeV, decreasing below 1° for energies above 1 GeV (Chen et al. 2013), an unprecedentedly large field of view (FOV) of about ~ 2.5 sr, as well as accurate timing, positional and attitude information (source location accuracy $5'–10'$ for intense sources with $S/N \geq 10$).

4. AGILE data set

During its first period of data taking (about two years) the AGILE satellite was operated in “pointing observing mode”,

² <http://www.asdc.asi.it/tgevcats/>

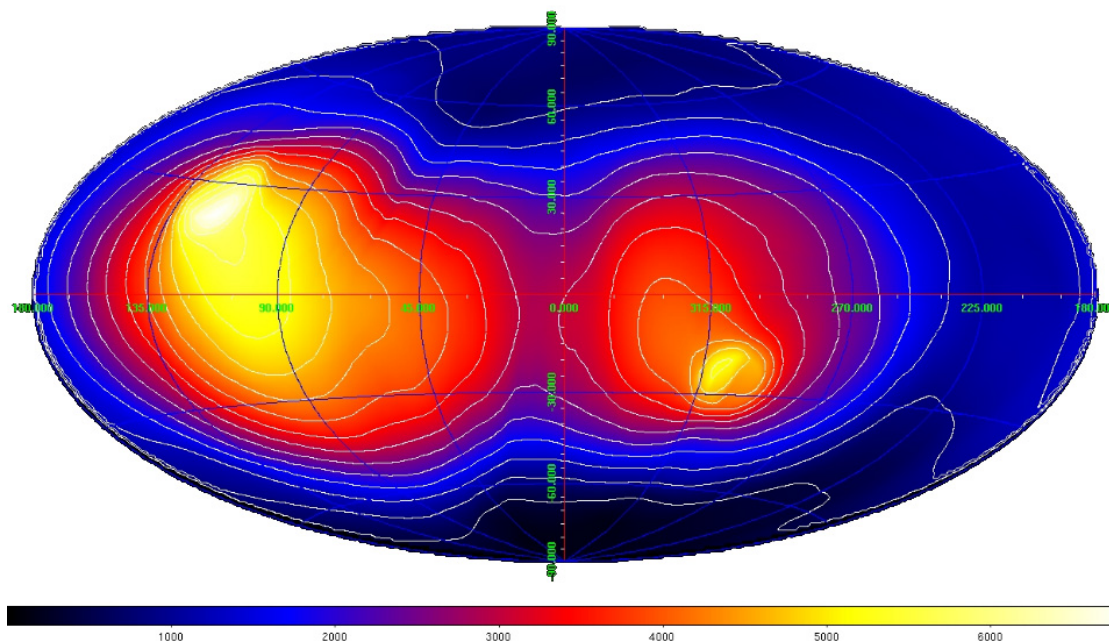


Fig. 2. Total AGILE exposure map during the first ~two years of operations (July 2007–October 2009). The exposure values are expressed in [$\text{cm}^2 \text{Ms}$]. The mean, maximum and minimum exposures attained correspond to values of about 2250, 6800, and 60 $\text{cm}^2 \text{Ms}$, respectively.

and the corresponding AGILE data are divided into observation blocks (OBs). Each AGILE OB consists of long exposures, which mostly range from a few days to about thirty days, with the pointing direction drifting $\sim 1^\circ$ per day with respect to the initial boresight direction to match solar panel illumination constraints.

The analysed AGILE data set covers the period from July 9, 2007 (beginning of the science verification phase) to October 18, 2009, corresponding to 96 OBs (not including the first five OBs of the Commissioning). During this period, following the main scientific program of the AGILE mission, the satellite was mainly pointed to observe two regions near the Galactic plane, around $l = 90^\circ$ and $l = 270^\circ$ longitude values, as shown by the total exposure map in Fig. 2. Clearly, this observation strategy mainly focused on the Galactic plane was not optimal for detecting extragalactic TeV sources.

5. Data analysis procedure

An iterative automated procedure has been developed to analyse the entire pointing AGILE data set described in Sect. 4, searching for possible γ -ray excesses correlated to the TeV sources. For each TeV source in the reference sample that is defined in Sect. 2, this procedure is divided in two main parts.

5.1. Map creation

The first part consists in the creation of the maps of counts, exposure and diffuse γ -ray background based on the model described in (Giuliani et al. 2004), updated together with the new GRID calibrations, which are centred at the TeV source position, over the full AGILE pointed observation period. These maps are in Galactic coordinates (l, b), ARC projection, with a size of $40^\circ \times 40^\circ$ divided into bins of $0.1^\circ \times 0.1^\circ$, and they have been produced using the latest official AGILE scientific analysis software (Chen et al. 2011) – available at ASDC – with the following parameters:

- data archive: ASDCSTDe

- initial time: MJD (TT) = 54 290.5 (MET=111067134 s)³
- final time: MJD (TT) = 55 122.5 (MET=182951934 s)
- energy range: 100 MeV ÷ 50 GeV
- software release: BUILD21
- event filter: FM3.119
- response matrices: l0023.

The event filter is the algorithm that processes the GRID raw data and reconstructs the energy and direction of the incident γ -ray in the GRID reference system. The event filter used in this analysis (FM3.119) represents the most updated reconstruction algorithm, which provides a good trade-off between FoV, effective area, and background rejection (Chen et al. 2011, 2013). Maps were generated for energies $E > 100$ MeV, including all events collected up to 60° off-axis. The South Atlantic Anomaly data were excluded and, to eliminate the Earth albedo contamination, events with reconstructed directions with respect to the satellite-Earth vector that were smaller than 85° were also rejected.

5.2. Source detection

The next part of the automatic procedure consists in verifying if, around the input TeV position, it is possible to detect the presence of a significant γ -ray source and, if so, to try to locate the best position of the γ -ray excess.

The source detection is performed by means of a multi-source maximum likelihood estimator (MLE) algorithm that estimates the photon counts and the position of the TeV source, the expected contribution given by the background components (modelled as a superposition of a Galactic diffuse emission background and an isotropic component), all the known AGILE γ -ray sources within the region of analysis, also taking into account the instrument response function.

³ MET is the AGILE Mission Elapsed Time in seconds since 2004.0 UTC.

In particular, the MLE analysis was performed taking into account all the known γ -ray sources detected by AGILE at the time of the analysis, consisting of a set of 65 sources, which were obtained by combining the 54 sources of the updated list of AGILE bright sources (1AGLR; Verrecchia et al. 2013), plus 11 sources not bright enough to be detected over the short OB time scales of the 1AGLR analysis: i.e. eight 1AGL sources from the first AGILE high confidence catalog (Pittori et al. 2009) and two AGL sources in the Carina region (see also Tables 2 and 3 of 1AGLR paper), plus one additional AGL source from a detailed analysis of the Cygnus region (Bulgarelli et al. 2012b). All AGILE sources are assumed to be point-like with simple power-law spectra.

With the exception of bright sources (significance >5), AGILE data analysis may not be spectrally resolved owing to low statistics and, in general, a standard fixed spectral index value of -2.1 is adopted for the initial steps of the ML analysis. This assumption is motivated by the known spectral properties of the majority of the γ -ray sources in the AGILE energy range, except for a few sources, as described in the 1AGLR. Timing analysis of pulsars was not performed in this paper, and the γ -ray emission that is detected in the search of counterparts to the TeV emission from PWN is, in general, due to the average (pulsar + nebula) γ -ray flux values.

The significance of a source detection is evaluated by the square root of the test statistic TS , defined as

$$TS = -2 \log \left(\frac{\mathcal{L}_0}{\mathcal{L}_1} \right) \quad (1)$$

where $\mathcal{L}_0/\mathcal{L}_1$ is the ratio between the maximum likelihood \mathcal{L}_0 of the null hypothesis and the likelihood \mathcal{L}_1 of the alternative hypothesis (presence of a point-like source under evaluation; Mattox et al. 1996; Bulgarelli et al. 2012a). For a large enough number of counts ($N \gtrsim 20$), TS is expected to behave as χ^2_1 in the null hypothesis, and the significance of a source detection is given by \sqrt{TS} .

The source detection algorithm is very flexible and can be used with a variety of parameters and options that allow us to refine the process of source detection and location. For example, both the position and the flux of the analysed source can be considered fixed or variable (starting from a defined initial value). Additionally, the coefficients of the Galactic background (diffuse emission and isotropic component) may in turn be kept fixed or treated as variable.

To get the best result for the position and flux estimation of the analysed sources, an iterative MLE analysis is performed, divided into the following steps:

- *Step 1*: the aim of the first step is both to find an excess of γ -rays around the input TeV source position in the AGILE data and to estimate, by the minimisation algorithm, the best values of the γ -ray background model parameters (galactic and extragalactic isotropic contributions). The MLE analysis is performed allowing the source coordinates to vary within a distance $\leq 1^\circ$ from the input TeV source position, taking all known AGILE sources in the region of analysis with a radius of 10° into account;
- *Step 2*: in this step the γ -ray excess position is refined by fixing the Galactic background coefficients to the best values obtained from Step 1;
- *Step 3*: this is the final step to estimate the flux and significance $\sqrt{(TS)_3}$ of the γ -ray source at the optimised position,

which results from Step 2, using updated Galactic background coefficients at the new position;

- *Step 4*: this step gives directly an estimation of the flux and significance $\sqrt{(TS)_4}$ of the γ -ray source, assuming a fixed position that is coincident with that of the input TeV source. In this case the diffuse background coefficients are estimated at the original input position.

Step 4 represents the standard method used in literature to verify the significance of known sources at input positions that are already known in other wavelengths. However, especially in the analysis of crowded regions of the Galactic plane, it is important also to search for a possible optimised position of the γ -ray excess, which is still compatible with the TeV source spatial association. This search is performed in *Steps 1–3*.

The possible shift in the γ -ray excess position may be due to several factors:

- the rather poor angular resolution of the order of a few degrees in the MeV–GeV energy range⁴;
- the AGILE reference catalog’s positioning errors (ranging from $\sim 0.1^\circ$ for very bright sources up to 0.7° for faint sources, at 95% CL);
- extended TeV source (X);
- the possible physical displacement between the TeV and the MeV–GeV emission regions.

In this paper an AGILE “detection” is in general defined by the condition

$$\sqrt{(TS)_4} \geq 4 \quad (2)$$

which corresponds to a statistical significance of about 4σ at the input TeV source position.

The search for optimised positions of the γ -ray excess gives results that are considered reliable when the MLE analysis (*Steps 1–3*) converges well within the allowed searching distance from the input position, and the significance of the detection is increased. In practice (see next section) this occurs when the following condition is satisfied:

$$\sqrt{(TS)_3} \geq 4 \text{ and } \text{dist} \lesssim 0.6^\circ \quad (3)$$

where *dist* is the angular distance between the position of the input TeV source and the candidate γ -ray source.

6. Results

In Table A.1, the complete list of all the TeV sources considered in this analysis is reported, showing the following relevant source parameters:

- ID: identification number;
- TeV source: TeV source name;
- (l,b): position of the TeV source in Galactic coordinates;
- TeV pos. err.: positional error of the input TeV source (derived as explained in Sect. 2);
- Canonical name;
- Type: type of TeV source counterpart, if already known from other wavelengths;
- $\sqrt{(TS)_4}$: estimate of the γ -ray statistical significance at *Step 4*;

⁴ About 0.7° PSF HWHM at 400 MeV, corresponding to the AGILE effective area peak values (Sabatini et al. 2015).

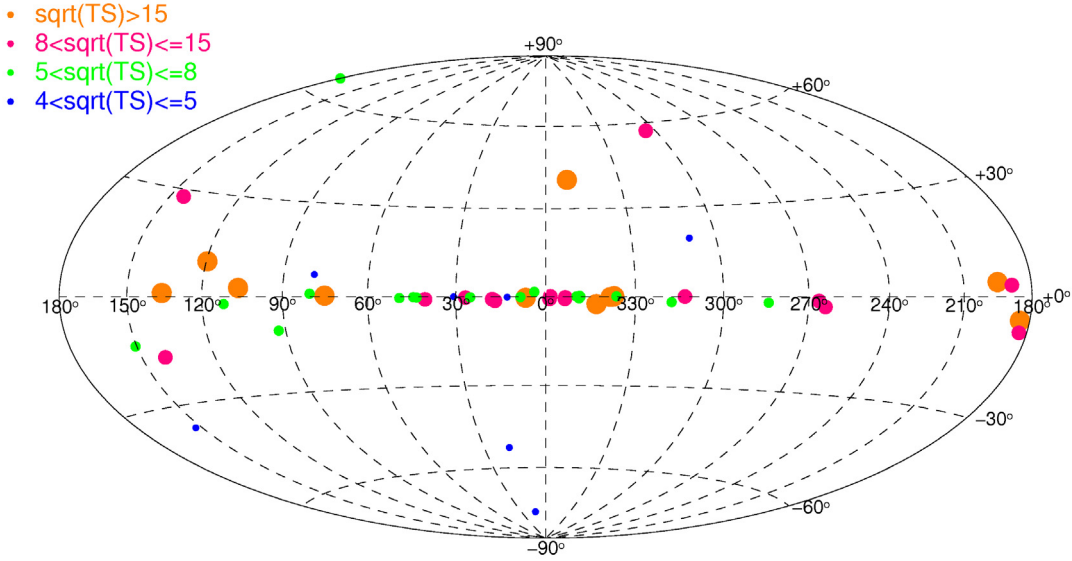


Fig. 3. Aitoff map in Galactic coordinates of all the detections according to the criteria specified in the text, corresponding to TeV sources that show a significant excess in the AGILE data.

- $\sqrt{(TS)_3}$: estimate of the γ -ray statistical significance at *Step 3*;
- Flux₄: estimate of the γ -ray flux ($E > 100$ MeV) and its 1σ statistical error in units of 10^{-7} ph cm $^{-2}$ s $^{-1}$, for AGILE detected sources at the input TeV source position from *Step 4*;
- UL₄: AGILE γ -ray flux upper limit at 95% confidence level (CL) at the input TeV source position from *Step 4*;
- EXT: TeV source extension.

In Table A.1, the γ -ray sources detected according to the criteria specified in Sect. 5.2 are shown in bold. For these sources the calculated flux value and the corresponding error is given, while for the sources not satisfying the detection requirement, the estimated 95% CL upper limit is reported.

In total, 52 TeV sources show a significant excess in the AGILE data that covers the pointed observation period, corresponding to 34% of the original sample. The Aitoff map in Galactic coordinates of all the detections is shown in Fig. 3.

Table A.2 groups all the sources detected with AGILE in this work (shown in bold in the previous table), and it includes the following columns:

- ID: source identification number used in Table A.1
- TeV source: TeV source name;
- $\sqrt{(TS)}$: estimate of the γ -ray source statistical significance as result of the AGILE MLE analysis (upper part *Step 3*, lower part *Step 4*);
- (l,b): optimised peak position of the AGILE excess in Galactic coordinates (upper part);
- Error: γ -ray source location error radius at 95% CL from *Step 3* (statistical error only);
- Flux: estimate of the γ -ray flux ($E > 100$ MeV) at the optimised peak position and its 1σ statistical error in units of 10^{-7} ph cm $^{-2}$ s $^{-1}$;
- Dist: distance of the γ -ray peak position from the input position of the TeV source;
- AGILE association: already known AGILE source from the published 1AGL/1AGLR catalogs (Pittori et al. 2009; Verrecchia et al. 2013) within the error radius in the 7th column;

- Fermi association: known *Fermi*-LAT source(s) associated to the TeV source, as described on 3FGL catalog (Acero et al. 2015);
- Analysis flag (see below).

Table A.2 is split into two sections: the upper part reports the results of the MLE analysis *Step 3* for all the sources that satisfy the condition in Eq. (3). The lower part includes the detected sources that satisfy the condition in Eq. (2) but not Eq. (3), for which the *Step 3* automatic analysis is not reliable. For this reason, the values of \sqrt{TS} and flux shown in this part of the table are those found at *Step 4* at the input TeV positions. There are few exceptions to these criteria which are described in the table footnotes. For all of the 19 sources in the lower section of Table A.2, although the MLE analysis result at fixed input position is significant, the tentative optimisation of the location of the γ -ray peak flux fails. In these cases the region of analysis may not yet be well modelled, and a refined MLE analysis should be performed after the release of a new AGILE catalog (Bulgarelli et al., in prep.).

As reported in the 8th column of Table A.2, 26 spatial associations of the detected TeV sources with already known AGILE sources from the 1AGL/1AGLR catalogs are found within the 95% CL error radius (7th column; Pittori et al. 2009; Verrecchia et al. 2013). Among these sources, 15 are galactic, six are extragalactic and five are unassociated. As reported in the 9th column, 46 spatial associations with known Fermi sources from the 3FGL catalog are found (we note that some TeV sources have more than one 3FGL association). Fermi counterparts that are officially associated to the corresponding TeV source in the 3FGL catalog may have flag P (for point-like sources) or E (for extended sources).

Column 10th of Table A.2 reports an analysis flag assigned to the AGILE detection according to the position and extent of the source location contour:

- IN (Inside): the TeV source, including its extension (if any), is entirely within the AGILE contour (see an example in Fig. 4);

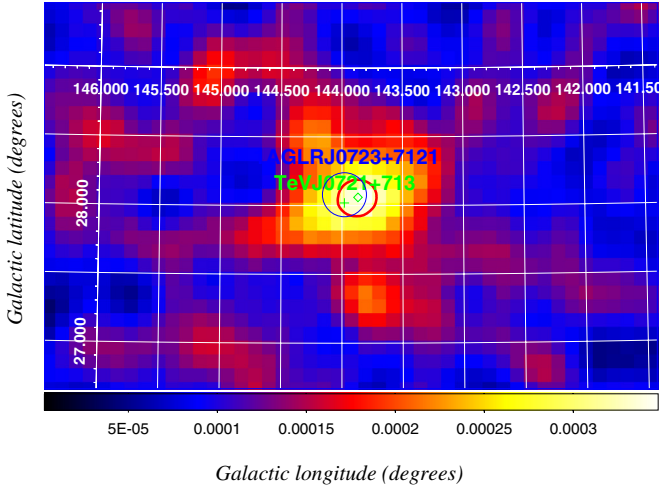


Fig. 4. Source detection in the position of TeV J0721+713. The signal is detected with $\sqrt{(TS)_3} = 13.9$, and the localization algorithm gives the 95% CL contour (red curve) that entirely contains the TeV source position (green cross). The AGILE counterpart 1AGLR J0723+7121 is also shown with its error radius (blue circle). The image shows the intensity map ($\text{cm}^{-2} \text{s}^{-1} \text{bin}^{-1}$) in Galactic coordinates, with bin size $0.1^\circ \times 0.1^\circ$ and Gaussian smoothing of three bins' radius.

- O (Overlapping): the AGILE contour at the 95% CL overlaps with the error circle and/or the extension of the TeV source (see Fig. 5);
- E (External): the AGILE contour neither includes nor overlaps with the TeV source. Nevertheless, the AGILE peak position is within 0.6° from the TeV source position (see Fig. 6).

In this work, 26 new AGILE sources are found with respect to the AGILE reference catalogs, 15 of which are galactic, 7 are extragalactic and 4 are unidentified. Detailed statistics about the type of the detected source can be found in Table A.4.

Eight sources are detected by AGILE in this analysis with no Fermi 3FGL official association:

- * ID 88: TeV J1634-472 (HESS J1634-472)
- ID 96: TeV J1713-382 (CTB 37B)
- ID 103: TeV J1729-345 (HESS J1729-345)
- ID 104: TeV J1732-347 (HESS J1731-347)
- ID 105: TeV J1741-302 (HESS J1741-302)
- * ID 116: TeV J1813-178 (HESS J1813-178)
- ID 133: TeV J1911+090 (W49B)
- ID 134: TeV J1912+101 (HESS J1912+101)

two of which, indicated by asterisks, have counterparts in the already published AGILE catalogs, and do not represent new detections.

6.1. Spectral analysis

Table A.3 shows the results of the spectral analysis performed on the most significant sources detected in this analysis. Only the 24 sources detected with a significance $\sqrt{(TS)_3} > 5$ (see Table A.2, upper part) and $|b| < 30^\circ$ have been considered.

For all considered sources, the AGILE spectral index shown in the fourth column of Table A.3 has been calculated generating exposure, counts and diffuse background maps over five energy bands: 100–200 MeV, 200–400 MeV, 400–1000 MeV,

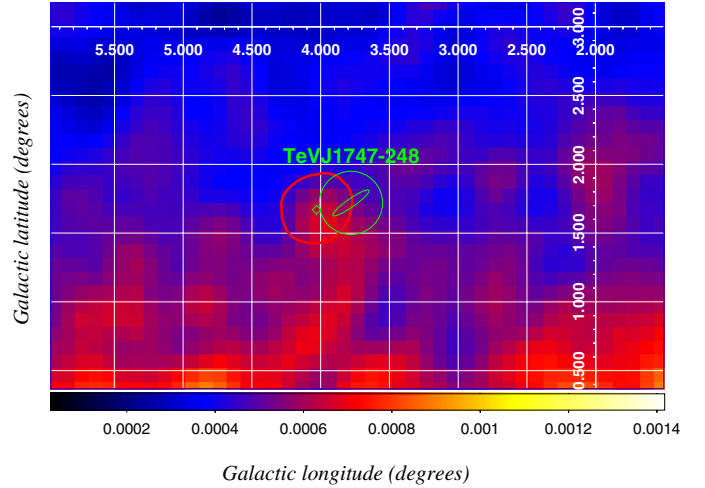


Fig. 5. Source detection in the position of TeV J1747-248. The signal is detected with $\sqrt{(TS)_3} = 5.9$, and the localization algorithm gives the 95% CL contour (red curve) which partially overlaps with the error circle and the extension of the TeV source (green circle and green ellipse). The image shows the intensity map ($\text{cm}^{-2} \text{s}^{-1} \text{bin}^{-1}$) in Galactic coordinates, with bin size $0.1^\circ \times 0.1^\circ$ and Gaussian smoothing of three bins' radius.

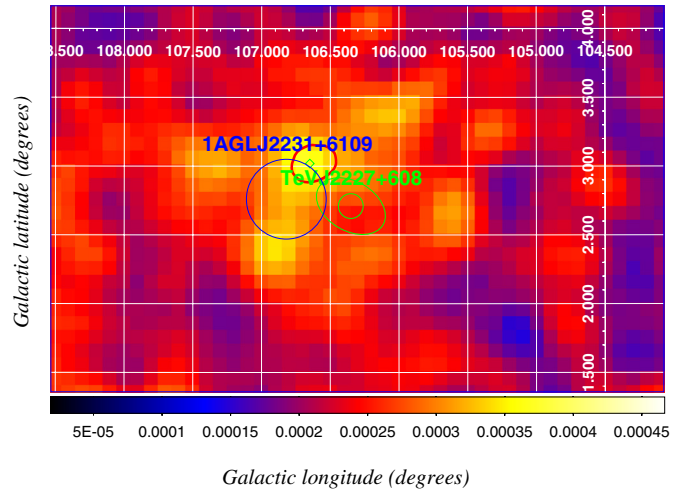


Fig. 6. Source detection in the position of TeV J2227+608. The signal is detected with $\sqrt{(TS)_3} = 16.7$, and the localization algorithm gives the 95% CL contour (red curve) which neither includes nor overlaps with the error circle and the extension of the TeV source (green circle and green ellipse). The AGILE counterpart 1AGL J2231+6109 is also shown with its error radius (blue circle). The image shows the intensity map ($\text{cm}^{-2} \text{s}^{-1} \text{bin}^{-1}$) in Galactic coordinates, with bin size $0.1^\circ \times 0.1^\circ$ and Gaussian smoothing of three bins' radius.

1–3 GeV, and 3–50 GeV, under the assumption of a power-law energy distribution.

For comparison, the Fermi power-law spectral index of the 3FGL counterpart of the TeV source is also shown in the last column of the table⁵. AGILE and Fermi power-law spectral indices are also compared in Fig. 7. A quantitative comparison between Fermi and AGILE power-law spectral indices can be done adding quadratically the AGILE and Fermi power-law spectral

⁵ The “power law index” reported in the 3FGL catalog (Acero et al. 2015) is given without error, and corresponds to the result of fitting the spectrum with a power-law function; it is equal to “spectral index” only when spectrum type is PowerLaw and in these cases errors are available.

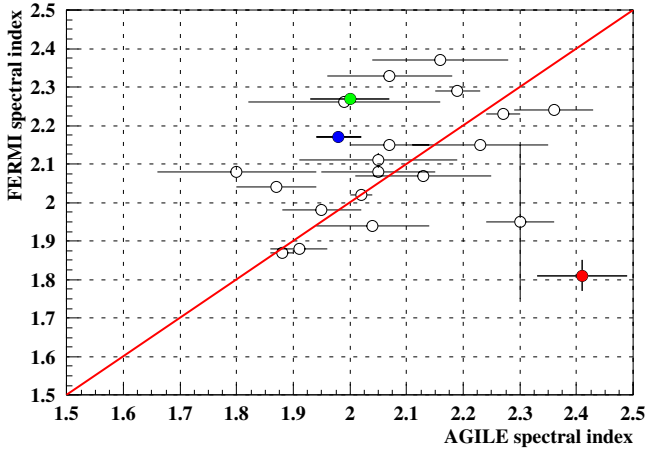


Fig. 7. Comparison between the spectral index evaluated for the most significant sources that were detected by AGILE, and the corresponding “power-law” spectral index reported by Fermi (22 sources). The horizontal bars represent the AGILE spectral index errors, the vertical bars represent the Fermi spectral index errors, when available. The coloured points refer to the sources highlighted in Fig. 8.

index errors when available or relying only on the AGILE error. No systematic error is assumed. Based on these very conservative assumptions, the distribution of the pulls (difference between the AGILE and Fermi power-law spectral indices divided by their combined errors) shown in Fig. 8 may be significantly overestimated. Nevertheless, for most of the sources (19 out of 22), AGILE and Fermi power-law spectral indices agree within three σ .

As explained in Sect. 5.2, the analysis in this paper was performed taking into account all the known γ -ray sources detected by AGILE at the time of the analysis, and in general more than one 3FGL source may be within the 95% AGILE error circle (plus a suggested systematic error of 0.1°). In particular, in the TeV J1841-055 case – the one with the largest pull (red) – there are three 3FGL sources within the AGILE detection error circle. The TeV source has an extension of the order of 0.5 deg, and the AGILE spectral result was compared with the associated extended Fermi PWN 3FGL J1840.9-0532e. It is likely that the other two γ -ray sources (3FGL J1839.3-0552 and 3FGL J1838.9-0537) contribute to the AGILE-detected emission, both having softer power-law spectral indices.

7. Conclusions and discussion

An analysis has been performed on a sample of 152 known TeV sources using the first two years of AGILE data with the purpose of detecting γ -ray emission that is associated with these TeV sources⁶.

A significant γ -ray excess in the AGILE data has been found for 52 input TeV sources, corresponding to $\sim 34\%$ of the analysed sample. In particular, 26 new AGILE sources have been found with respect to the AGILE reference catalogs, 15 of which are galactic, seven are extragalactic and four are unidentified.

Eight of the AGILE detected TeV sources (listed in Sect. 6) have no 3FGL official association and will be further investigated in a dedicated paper.

⁶ An interactive online version of the source list including all the analysis results is also accessible at the ASDC website <http://www.asdc.asi.it/agiletevcats/>

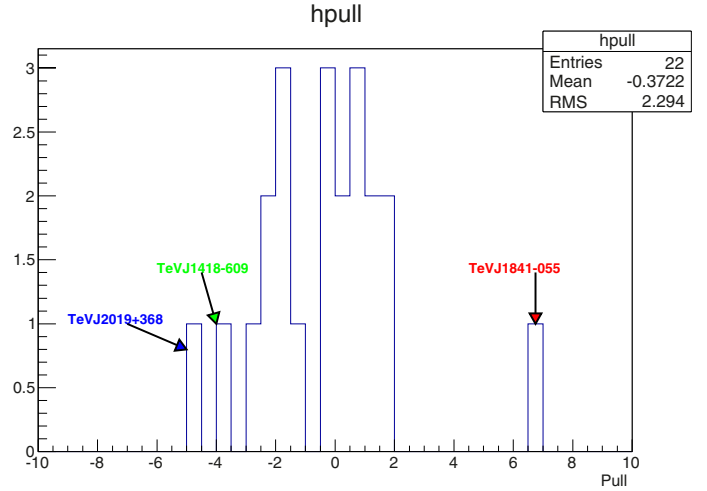


Fig. 8. Pull distribution of the difference between the AGILE and Fermi power-law spectral indices divided by their combined errors. The three sources with pull larger than three are shown.

The difference between the two experiments in some cases may be due to a different response to softer spectral index sources with spectral energy distribution peaking in the 100–400 MeV energy range or to differences in the assumed background diffuse model. A new Fermi analysis using the recently delivered Pass 8 Data, which provides a significant increase in acceptance at lower energies may result in new Fermi associations. Furthermore according to the official Fermi collaboration association procedure, only counterparts which reach a posteriori probability of at least 80% are retained, and this does not mean that there is no 3FGL source within the error region.

The spatial association of a TeV source with an AGILE source may be due to chance. The probability of a serendipitous association may be estimated by evaluating the total sky coverage of all catalogued AGILE sources, which are defined by their 95% error radius, and then calculating the overall probability that each TeV source can overlap to any AGILE source, that is, the distance between a TeV source and an AGILE source is, by chance, smaller than the sum of their error circles (Funk et al. 2007). Because the density of both TeV and AGILE sources are strongly non-uniform, being much larger on the Galactic plane, this evaluation is performed separately on a narrow stripe along the Galactic plane⁷, defined by $|b| \leq 3^\circ$, and on all the rest of the sky map, defined by $|b| > 3^\circ$. The number of serendipitous associations is found to be 0.82 for this type of band around the Galactic plane, whereas it is 0.08 for the other region. Therefore the chance coincidence should be $O(1)$ over the whole sky.

The analysis that we have accomplished and described in this paper concerns a nearly continuous data taking period of about two year, therefore the obtained fluxes (and corresponding detection significances) are the average values integrated over a rather long time. For this reason, some γ -sources that are characterised by high variability (for example W Comae (Verrecchia et al. 2008) and 4C +21.35 Bulgarelli et al. 2010; Striani et al. 2010; Verrecchia et al. 2014) have not been detected in this analysis (and similarly in Verrecchia et al. 2013), even if they have already been detected and analysed in other previous observations published by AGILE, which refers to shorter time periods in coincidence with their flares.

⁷ The probability estimation is weakly dependent on the boundary used.

The majority of the AGILE detected sources are galactic. This might be a bias due the higher exposure of the Galactic plane during the pointing period, see Fig. 2.

From the Analysis flag reported in Table A.2, 13 AGILE detected sources in the Galactic plane are flagged as “overlapping” or “external” with the TeV emission region. This may indicate a possible displacement between the TeV and the GeV emission regions, as is the case for the IC443 SNR (Tavani et al. 2010).

Acknowledgements. The authors would like to thank the Istituto Nazionale di Astrofisica, the Agenzia Spaziale Italiana, the Consorzio Interuniversitario per la Fisica Spaziale, and the Istituto Nazionale di Fisica Nucleare for their generous support of the AGILE mission and this research, including ASI contracts N. I/042/10/1 and I/028/12/0.

References

- Abdo, A. A., Ackermann, M., Ajello, M., et al. 2009, *ApJ*, 707, 1310
- Acero, F., Ackermann, M., Ajello, M., et al. 2013, *ApJ*, 773, 77
- Acero, F., Ackermann, M., Ajello, M., et al. 2015, *ApJS*, 218, 23
- Bulgarelli, A., Gianotti, F., Trifoglio, M., et al. 2010, *ATel*, 2641, 1
- Bulgarelli, A., Chen, A. W., Tavani, M., et al. 2012a, *A&A*, 540, A79
- Bulgarelli, A., Tavani, M., Chen, A. W., et al. 2012b, *A&A*, 538, A63
- Carosi, A., Lucarelli, F., & Antonelli, L. 2015, in Proc. 34th International Cosmic Ray Conference, The Hague, The Netherlands, in press
- Chen, A. W., Argan, A., Bulgarelli, A., et al. 2013, *A&A*, 558, A37
- Chen, A. W., et al. 2011, GRID Scientific Analysis – USER MANUAL, http://agile.asdc.asi.it/public/AGILE_SW_5.0_SourceCode/
- Ferenc, D. 2005, *Nucl. Instrum. Methods A*, 553, 274
- Funk, S., Reimer, O., Torres, D., & Hinton, J. A. 2007, in Proc., 30th International Cosmic Ray Conference, 2, 617
- Funk, S., Reimer, O., Torres, D. F., & Hinton, J. A. 2008, *ApJ*, 679, 1299
- Funk, S., Hinton, J. A., & CTA Consortium. 2013, *Astropart. Phys.*, 43, 348
- Giuliani, A., Chen, A. W., & Mereghetti, S. 2004, *Mem. Soc. Astron. It. Supp.*, 5, 135
- Hinton, J. 2004, *New Astron. Rev.*, 48, 331
- Holder, J., Atkins, R. W., Badran, H. M., et al. 2006, *Astropart. Phys.*, 25, 391
- Longo, F., Rappoldi, A., Lucarelli, F., et al. 2011, TeV sources analysis with AGILE, arXiv e-print [[arXiv:1111.2039](https://arxiv.org/abs/1111.2039)]
- Lucarelli, F., Pittori, C., Rappoldi, A., & Longo, F. 2011, in 32nd International Cosmic Ray Conference, Beijing, China, 7, 236
- Mattox, J., Bertsch, D., Chiang, J., et al. 1996, *ApJ*, 461, 396
- Pellizzoni, A., Trois, A., Tavani, M., et al. 2010, *Science*, 327, 663
- Pittori, C., Verrecchia, F., Chen, A. W., et al. 2009, *A&A*, 506, 1563
- Rappoldi, A., Longo, F., Argan, A., et al. 2011, *Nucl. Instrum. Methods A*, 630, 202
- Sabatini, S., Donnarumma, I., Tavani, M., et al. 2015, *ApJ*, 809, 60
- Striani, E., Verrecchia, F., Donnarumma, I., et al. 2010, *ATel*, 2686, 1
- Tavani, M., Barbiellini, G., Argan, A., et al. 2009, *A&A*, 502, 995
- Tavani, M., Giuliani, A., Chen, A. W., et al. 2010, *ApJ*, 710, L151
- Verrecchia, F., Gasparrini, D., Cutini, S., et al. 2008, *ATel*, 1582, 1
- Verrecchia, F., Pittori, C., Chen, A. W., et al. 2013, *A&A*, 558, A137
- Verrecchia, F., Lucarelli, F., Pittori, C., et al. 2014, *ATel*, 6733, 1

Appendix A: Additional tables

Table A.1. 152 TeV sources considered in this analysis.

ID	TeV source	(<i>l</i> , <i>b</i>) [deg] ⁹	TeV pos. err. [deg]	Canonical name	Type ⁸	$\sqrt{(TS)^4}$	$\sqrt{(TS)^3}$	Flux _{X4} (<i>E</i> > 100 MeV) [10 ⁻⁷ ph cm ⁻² s ⁻¹]	UL ₄ [10 ⁻⁷ ph cm ⁻² s ⁻¹]	Ext.
1	TeVJ0006+727	119.604, 10.403	0.091	CTA 1	PWN/SNR	21.4	21.6	3.3 ± 0.2		X
2	TeVJ0013-189	74.6130, -78.0684	0.0083	SHBL J001355.9-185406	HBL				1.5	
3	TeVJ0025+640	120.106, 1.451	0.026	Tycho SN, G120.1+1.4	SNR	1.6	1.6		0.7	
4	TeVJ0033-193	94.171, -81.216*	-	KUV 00311-1938	HBL				2.0	
5	TeVJ0035+598	120.898, -3.018	0.030	IES 0033+595	HBL				0.2	
6	TeVJ0047-253	97.4696, -87.9672	0.0080	NGC 253	Sbs				0.6	
7	TeVJ0112+227	129.14, -39.88*	-	S2 0109+22	IBL	1.8	3.3		0.8	
8	TeVJ0136+391	132.416, -22.940*	-	RGB J0136+391	HBL	1.2	1.2		0.5	
9	TeVJ0152+017	152.343, -57.561	0.030	RGB J0152+017	HBL	1.9	3.7		1.5	
10	TeVJ0209+648	130.701, 3.102	0.059	3C 58	PWN	2.1	4.8		0.8	
11	TeVJ0218+359	142.602, -23.487	-	S3 0218+35	AGN	3.3	3.9		1.0	
12	TeVJ0222+430¹⁰	140.143, -16.767	-	3C 66A	IBL	8.0	8.1	1.4 ± 0.2		
13	TeVJ0223+430 ¹⁰	140.254, -16.772	0.048	MAGIC J0223+430	UNID	7.6	8.0	1.3 ± 0.2		
14	TeVJ0232+202	152.970, -36.613	0.014	IES 0229+200	HBL	3.1	4.2	0.9 ± 0.3		
15	TeVJ0240+612	135.668, 1.113	0.034	LSI+61_303	XR	26.7	27.0	6.5 ± 0.3		
16	TeVJ0303-241	214.6296, -60.1899	0.0073	PKS 0301-243	HBL				0.9	
17	TeVJ0316+413	150.183, -13.734	-	IC 310	HBL				0.3	
18	TeVJ0319+187	165.088, -31.708*	0.034	RBS 0413	HBL	2.0			1.2	
19	TeVJ0319+415	150.576, -13.261	-	NGC 1275	FRI	5.5	5.5	1.0 ± 0.2		
20	TeVJ0349-119	201.909, -45.704	0.011	IES 0347-121	HBL				0.8	
21	TeVJ0416+010	191.8167, -33.1581	0.0069	IES 0414+009	HBL	2.4	3.4		1.5	
22	TeVJ0449-438	248.8066, -39.9082	0.0072	PKS 0447-439	HBL	1.3	1.3		1.1	
23	TeVJ0507+676	143.795, 15.890*	-	IES 0502+675	HBL				0.2	
24	TeVJ0521+211¹¹	183.6021, -8.7114	0.0080	RGB J0521.8+211	IBL	4.5	4.7	1.6 ± 0.4		
25	TeVJ0525-696	280.307, -32.784*	-	LMC N132D	SNR/MC	1.0	1.0		0.6	
26	TeVJ0534+220	184.5558, -5.7870	0.0070	Crab Nebula	PWN	55.7	55.9	26.7 ± 0.7		
27	TeVJ0535-692	279.60, -31.91	0.022	30 Dor C	Superbubble	3.5	3.8		1.1	

Notes. The sources passing the detection criteria discussed in Sect. 5.2 are shown in bold. For a detailed description of the table columns please refer to the text. ⁽⁸⁾ TeV source classification types: PWN: Pulsar Wind Nebulae; BIN: Binary; SNR: SuperNova Remnant; Sbs: Starbursts; UNID: UNIDentified; FSRQ: Flat Spectrum Radio Quasar; HBL: High frequency peaked BL Lac object; IBL: Intermediate frequency peaked BL Lac object; LBL: Low frequency peaked BL Lac object; XR: X-Rays Binary; WR: Wolf-Rayet star; FRI: Fanaroff-Riley type I; GC: Globular Cluster; MC: Molecular Cloud; PSR: Pulsar. Note that the γ -ray emission detected in the search of counterparts to the TeV emission from PWN is in general due to the average (pulsar + nebula) γ -ray flux values. Timing analysis of pulsars was not performed in this paper. ⁽⁹⁾ The * indicates that the best-fit position of the TeV excess is not available and the position of the optical/radio known counterpart has been used. ⁽¹⁰⁾ The sources TeVJ0222+430 and TeVJ0223+430 are as close as 0.1° and therefore indistinguishable in this analysis. Their detection is counted as one. ⁽¹¹⁾ Results of a refined MLE analysis performed using the updated AGILE best-fit position of the Crab Nebula (one of the known γ -ray sources within 10 deg from the TeV J0521+211 position) obtained in this work. ⁽¹²⁾ The TeV error region for the Vela X PWN does not overlap the AGILE Vela Pulsar position error, hence the Vela PSR average γ -ray flux value for a spectral index of -1.69 was subtracted in the MLE automatic analysis. However the result is affected by the very intense Vela Pulsar nearby. The Vela X accurate γ -ray flux estimate and source location by AGILE is discussed in the dedicated analysis in (Pelizzoni et al. 2010). ⁽¹³⁾ Also in this case, the MLE automatic analysis is affected by the very intense Vela Pulsar nearby. A dedicated analysis will be performed. ⁽¹⁴⁾ Detected by AGILE during a flaring episode (Verrecchia et al. 2008). ⁽¹⁵⁾ Detected by AGILE during several flaring episodes (Bulgarelli et al. 2010; Striani et al. 2010; Verrecchia et al. 2014). ⁽¹⁶⁾ The region of the MLE analysis is not well modelled since this source shows a point-like core and extended emission from the lobes, which are not yet included in the AGILE reference catalogs. A dedicated analysis will be performed. ⁽¹⁷⁾ AGILE detection presented at the 32nd ICRC (Lucarelli et al. 2011). ⁽¹⁸⁾ Source located in a crowded region of the Galactic plane. The automatic MLE analysis is not reliable. A dedicated analysis will be performed. ⁽¹⁹⁾ Source located in the region near the Galactic Center. The automatic MLE analysis is not reliable. A dedicated analysis is being performed with an improved AGILE diffuse background model in the Galactic center region (Fioretti et al., in prep.).

Table A.1. continued.

ID	TeV source	(<i>l</i> , <i>b</i>) [deg] ¹⁰	TeV pos. err. [deg]	Canonical name	Type	$\sqrt{(TS)^4}$	$\sqrt{(TS)^3}$	Flux ₄ (<i>E</i> > 100 MeV) [10 ⁻⁷ ph cm ⁻² s ⁻¹]	UL ₄ [10 ⁻⁷ ph cm ⁻² s ⁻¹]	Ext.
28	TeVJ0537-691	279.553, -31.750	0.010	N 157B	PWN	3.4	3.7		1.1	
29	TeVJ0550-322	237.562, -26.152	0.014	PKS 0548-322	HBL				0.6	
30	TeVJ0616+225	189.073, 2.918	0.085	IC 443	SNR	12.9	13.2	5.0 ± 0.5		X
31	TeVJ0632+057	205.660, -1.441	0.010	HESS J0632+057	XRB	2.5	4.8		1.9	
32	TeVJ0632+173	195.34, 3.78	0.50	Geminga PWN	PWN	75.2	82.6	40.3 ± 0.9		X
33	TeVJ0648+152	198.99, 6.32	0.12	RX J0648.7+1516	HBL				0.7	
34	TeVJ0650+250	190.282, 10.996*	-	IES 0647+250	HBL				0.6	
35	TeVJ0710+591	157.391, 25.421	0.027	RGB J0710+591	HBL				0.4	
36	TeVJ0721+713	143.981, 28.018*	-	S5 0716+714	LBL	13.8	13.9	2.6 ± 0.2		
37	TeVJ0809+523	166.246, 32.935	0.048	IES 0806+524	HBL	1.9	2.0		0.9	
38	TeVJ0835-455 ¹²	263.840, -3.073	0.034	Vela X	PWN	7.9	11.2	6.2 ± 0.8		X
39	TeVJ0847+115	215.456, 30.890*	-	RBS 0723	HBL				0.8	
40	TeVJ0852-463 ¹³	266.285, -1.241	-	RX J0852.0-4622	SNR	4.0	8.5	1.5 ± 0.4		X
41	TeVJ0955+696	141.409, 40.568*	-	M82	Sbs				0.3	
42	TeVJ0958+655	145.75, 43.13*	-	S4 0954+65	FSRQ	1.8	1.9		0.8	
43	TeVJ1010-313	266.896, 20.063	0.017	IRXS J101015.9-311909	HBL				0.1	
44	TeVJ1015+494	165.534, 52.712*	-	IES 1011+496	HBL	2.4	2.9		1.2	
45	TeVJ1018-589	284.256, -1.818	-	HSS J1018-589	BIN	7.0	7.9	2.4 ± 0.4		X
46	TeVJ1023-575	284.217, -0.401	0.030	Westerlund 2	WR	2.1	3.5		1.5	X
47	TeVJ1026-582	284.798, -0.520	0.090	HESS J1026-582	PWN				0.2	X
48	TeVJ1103-234	273.188, 33.074	0.012	IES 1101-232	HBL				0.3	
49	TeVJ1104+382	179.832, 65.032	-	Mrk 421	HBL	5.2	5.2	1.6 ± 0.4		X
50	TeVJ1119-614	292.102, -0.487	-	G 292.2-0.5	PWN	2.3	4.6		1.3	
51	TeVJ1136+676	133.453, 47.951*	-	RXJ1136.5+6737	HBL				0.4	
52	TeVJ1136+701	131.910, 45.641*	-	Mrk 180	HBL	1.4	1.4		0.7	
53	TeVJ1217+301	189.010, 82.046	0.016	IES 1215+303	HBL				0.3	
54	TeVJ1221+282 ¹⁴	201.734, 83.288	-	W Comae	IBL				1.0	
55	TeVJ1221+301	186.210, 82.743	0.031	IES 1218+304	HBL				0.2	
56	TeVJ1224+213 ¹⁵	255.074, 81.660*	-	4C +21.35	FSRQ	2.6	3.5		1.7	
57	TeVJ1224+246	233.952, 83.418	-	MS 1221.8+2452	HBL				0.7	
58	TeVJ1230+123	283.7388, 74.4946*	0.0080	M 87	FRI				1.0	
59	TeVJ1230+253	232.75, 84.91*	-	S3 1227+25	IBL	2.8	3.0		1.7	
60	TeVJ1256-057	305.104, 57.062*	-	3C 279	FSRQ	11.1	11.2	4.2 ± 0.5		
61	TeVJ1302-638	304.187, -0.987	0.011	PSR B1259-63	XRB				0.6	
62	TeVJ1303-631	304.213, -0.334	0.014	HESS J1303-631	PWN				0.4	X
63	TeVJ1315-426	307.540, 20.064	0.018	IES 1312-423	HBL	2.4	5.1		0.9	
64	TeVJ1325-430 ¹⁶	309.513, 19.425	0.021	Centaurus A	FRI	4.4	4.9	0.8 ± 0.2		X
65	TeVJ1356-645	309.812, -2.494	0.034	HESS J1356-645	PWN	1.7	2.0		1.0	X
66	TeVJ1418-609	313.247, 0.150	0.030	Kookaburra (Rabbit)	PWN	13.5	13.5	5.1 ± 0.4		X
67	TeVJ1420-607	313.558, 0.268	0.018	Kookaburra (PWN)	PWN				1.1	X
68	TeVJ1427+238	29.472, 68.208	0.033	PKS 1424+240	IBL	1.3	1.3		1.3	
69	TeVJ1427-608	314.408, -0.145	0.050	HESS J1427-608	UNID	1.2	1.2		1.1	X
70	TeVJ1428+426	77.487, 64.899*	-	H 1426+428	HBL				1.0	X
71	TeVJ1442-624	315.410, -2.300	0.059	RCW 86	SNR				0.5	X
72	TeVJ1443+120	8.330, 59.840*	-	IES 1440+122	IBL				0.6	
73	TeVJ1443+250	34.56, 64.70*	-	PKS 1441+25	FSRQ				0.7	
74	TeVJ1457-594	318.36, -0.43	0.14	G 318.2+0.1	SNR/MC				0.2	X

Table A.1. continued.

ID	TeV Source	(<i>l</i> , <i>b</i>) [deg] ¹⁰	TeV Pos. Err. [deg]	Canonical name	Type	$\sqrt{(TS)_4}$	$\sqrt{(TS)_3}$	Flux ₄ (<i>E</i> > 100 MeV) [10 ⁻⁷ ph cm ⁻² s ⁻¹]	UL ₄ [10 ⁻⁷ ph cm ⁻² s ⁻¹]	Ext.
75	TeVJ1459-608	317.748, -1.704	0.030	HESS J1458-608	PWN	5.6	5.8	1.5 ± 0.3		X
76	TeVJ1502-419	327.580, 14.571	-	SN 1006	SNR				0.3	
77	TeVJ1503-582	319.62, 0.29	0.10	HESS J1503-582	UNID				0.2	X
78	TeVJ1506-623	317.946, -3.494	0.050	HESS J1507-622	UNID	3.1	4.3		1.2	X
79	TeVJ1512-091	351.2907, 40.1296	0.0093	PKS 1510-089	FSRQ	24.8	25.0	8.1 ± 0.4		X
80	TeVJ1514-591	320.324, -1.200	0.010	MSH 15-52	PWN				0.6	X
81	TeVJ1517-243	340.673, 27.577*	0.014	AP Lib	LBL	2.0	3.6		0.8	X
82	TeVJ1554-550	327.158, -1.072	0.018	G 327.1-1.1	PWN				0.3	X
83	TeVJ1555+111	21.919, 43.960	0.016	PG 1553+113	HBL	1.9	4.4		1.3	X
84	TeVJ1614-518	331.52, -0.58	-	HESS J1614-518	UNID				0.8	X
85	TeVJ1616-508	332.39, -0.14	-	HESS J1616-508	PWN				0.9	X
86	TeVJ1626-490	334.772, 0.045	0.050	HESS J1626-490	UNID				0.3	X
87	TeVJ1632-478 ¹⁷	336.38, 0.19	-	HESS J1632-478	UNID	5.6	5.7	2.2 ± 0.4		X
88	TeVJ1634-472	337.11, 0.22	-	HESS J1634-472	UNID	15.4	15.7	6.3 ± 0.4		X
89	TeVJ1640-465	338.32, -0.02	-	HESS J1640-465	PWN	12.3	15.2	5.1 ± 0.5		X
90	TeVJ1641-463	338.519, 0.095	0.015	HESS J1641-463	UNID				1.0	X
91	TeVJ1647-458	339.55, -0.35	0.12	Westertund 1	WR	1.3	1.3		1.3	X
92	TeVJ1653+397	63.600, 38.859	-	Mrk 501	HBL	3.9	5.3		1.3	X
93	TeVJ1702-420	344.304, -0.184	0.050	HESS J1702-420	UNID				0.2	X
94	TeVJ1708-410	345.683, -0.469	0.050	HESS J1708-410	UNID				0.4	X
95	TeVJ1708-443	343.058, -2.376	0.071	HESS J1708-443	PWN/SNR	39.8	42.3	13.6 ± 0.4		X
96	TeVJ1713-382	348.639, 0.388	0.018	CTB 37B	SNR	6.5	7.8	2.6 ± 0.4		X
97	TeVJ1713-397	347.336, -0.473	-	RX J1713.7-3946	SNR	3.7	7.0		2.2	X
98	TeVJ1714-385 ¹⁸	348.389, 0.107	0.023	CTB 37A	SNR	7.0	7.5	2.8 ± 0.4		X
99	TeVJ1718-374	349.720, 0.174	0.010	G 349.7+0.2	SNR/MC	6.2	7.6	2.6 ± 0.4		X
100	TeVJ1718-385	348.834, -0.488	0.034	HESS J1718-385	PWN	6.9	7.5	2.7 ± 0.4		X
101	TeVJ1725+118	34.120, 24.475*	-	H 1722+119	HBL				0.4	
102	TeVJ1728+502	77.068, 33.537	-	IES 1727+502	HBL				0.4	
103	TeVJ1729-345	353.444, -0.128	0.035	HESS J1729-345	UNID	8.0	10.3	3.6 ± 0.5		X
104	TeVJ1732-347 ¹⁷	353.542, -0.670	-	HESS J1731-347	SNR	7.3	10.2	3.1 ± 0.5		X
105	TeVJ1741-302 ¹⁹	358.397, 0.191	-	HESS J1741-302	UNID	4.3	9.6	2.1 ± 0.5		X
106	TeVJ1743+196	43.836, 23.339*	-	IES 1741+196	HBL				0.3	
107	TeVJ1745-290	359.9449, -0.0440	0.0024	HESS J1745-290	UNID				0.3	
108	TeVJ1745-303	358.710, -0.640	-	HESS J1745-303	SNR/MC	11.2	12.7	5.5 ± 0.5		X
109	TeVJ1747-248	3.78, 1.72	0.45	Terzan 5	GC	5.2	5.9	1.9 ± 0.4		X
110	TeVJ1747-281	0.872, 0.076	-	G 0.9+0.1	PWN				0.1	
111	TeVJ1800-240	5.960, -0.380	0.044	HESS J1800-240 (A+B+C)	UNID				0.9	X
112	TeVJ1801-233	6.657, -0.268	0.032	W28	SNR/MC	14.0	15.0	6.5 ± 0.5		X
113	TeVJ1804-216	8.354, -0.000	-	HESS J1804-216	UNID	7.5	7.8	3.4 ± 0.5		X
114	TeVJ1808-204	9.960, -0.248	0.038	HESS J1808-204	UNID				1.3	
115	TeVJ1809-193	11.180, -0.088	0.050	HESS J1809-193	PWN	3.4	4.1	1.9 ± 0.5	2.4	X
116	TeVJ1813-178	12.812, -0.026	-	HESS J1813-178	PWN	4.1	4.8			X
117	TeVJ1818-154	15.409, 0.161	0.014	G 15.4+0.1	PWN	1.8	9.0		1.7	X
118	TeVJ1825-137	17.711, -0.697	0.018	HESS J1825-137	PWN	8.0	11.3	3.8 ± 0.5		X
119	TeVJ1826-148 ¹⁸	16.902, -1.278	0.012	LS 5039	XRB	7.7	10.7	3.3 ± 0.5		X
120	TeVJ1831-099	21.850, -0.109	-	HESS J1831-098	PWN	1.9	4.2		1.8	X
121	TeVJ1832-093	22.476, -0.177	0.015	G 22.7-0.2	SNR/MC	1.1	1.1		1.4	X

Table A.1. continued.

ID	TeV Source	(<i>l</i> , <i>b</i>) [deg] ¹⁰	TeV Pos. Err. [deg]	Canonical name	Type	$\sqrt{(TS)_4}$	$\sqrt{(TS)_3}$	Flux ₄ (<i>E</i> > 100 MeV) [10 ⁻⁷ ph cm ⁻² s ⁻¹]	UL ₄ [10 ⁻⁷ ph cm ⁻² s ⁻¹]	Ext.
122	TeVJ1833-106	21.511, -0.876	0.016	HESS J1833-105	UNID	2.3	3.6		1.8	
123	TeVJ1834-087	23.24, -0.32	-	HESS J1834-087	UNID				0.9	X
124	TeVJ1837-069	25.18, -0.11	-	HESS J1837-069	UNID	4.9	7.4	2.1 ± 0.4		X
125	TeVJ1841-055 ¹⁷	26.795, -0.198	0.050	HESS J1841-055	UNID	12.4	14.0	5.0 ± 0.4		X
126	TeVJ1843-030	29.033, 0.370	-	HESS J1843-033	UNID	3.6	6.7		2.2	
127	TeVJ1846-029	29.705, -0.240	0.011	HESS J1846-029	PWN	1.6	1.6		1.5	
128	TeVJ1848-017	31.000, -0.160	-	WR121a/W43	WR	3.7	4.6	1.4 ± 0.4		X
129	TeVJ1849-000	32.638, 0.526	-	IGR J18490-0000	PWN				1.0	
130	TeVJ1857+026	36.003, -0.061	0.039	HESS J1857+026	UNID				0.2	X
131	TeVJ1858+020	35.578, -0.581	0.050	HESS J1858+020	UNID				0.1	X
132	TeVJ1907+062	40.280, -0.688	0.020	MGRO J1908+06	UNID	12.9	13.3	4.5 ± 0.4		X
133	TeVJ1911+090	43.259, -0.189	0.071	W 49B	SNR/MC	7.6	7.8	2.4 ± 0.3		X
134	TeVJ1912+101	44.391, -0.071	0.050	HESS J1912+101	PWN	4.1	7.6	1.3 ± 0.3		X
135	TeVJ1923+141	49.116, -0.365	0.015	W 51	SNR/MC	7.0	7.1	2.1 ± 0.3		X
136	TeVJ1930+188	54.10, 0.26	0.11	G 54.1+0.3	PWN	3.5	5.2		1.5	
137	TeVJ1943+213	57.7577, -1.2928	0.0073	HESS J1943+213	HBL				0.5	
138	TeVJ1959+651	98.003, 17.670*	-	IES 1959+650	HBL	3.4	3.7		0.7	
139	TeVJ2001+438	79.071, 7.110	-	MAGIC J2001+435	HBL	4.9	4.8	0.9 ± 0.2		X
140	TeVJ2009-488	350.3741, -32.6052	0.0083	PKS 2005-489	HBL				0.4	
141	TeVJ2016+372	74.940, 1.140	0.019	VER J2016+372	UNID				0.3	
142	TeVJ2019+368	74.828, 0.417	0.090	MGRO J2019+37	PWN	24.7	25.5	6.7 ± 0.3		X
143	TeVJ2019+407	78.331, 2.489	0.035	VER J2019+407	UNID				0.1	X
144	TeVJ2032+415	80.279, 1.042	0.044	TeV J2032+4130	UNID	7.6	8.0	2.2 ± 0.3		X
145	TeVJ2158-302	17.737, -52.247	-	PKS 2155-304	HBL	4.6	4.8	1.3 ± 0.3		X
146	TeVJ2202+422	92.590, -10.441	-	BL Lacertae	LBL	7.2	8.0	1.0 ± 0.2		X
147	TeVJ2227+608	106.35, 2.71	0.10	G 106.3+2.7	SNR	15.2	16.7	3.0 ± 0.2		X
148	TeVJ2243+203	86.567, -33.365*	-	RGB J2243+203	HBL				0.4	
149	TeVJ2250+384	98.254, -18.578	-	B3 2247+381	HBL				0.2	
150	TeVJ2323+588	111.735, -2.130	0.020	Cassiopeia A	SNR	5.2	7.2	0.9 ± 0.2		X
151	TeVJ2347+517	112.73, -9.86	0.10	IES 2344+514	HBL				0.3	
152	TeVJ2359-306	12.8689, -78.0367	0.0086	H 2356-309	HBL	3.9	4.0	3.3 ± 1.0		X

Table A.2. Results for all the sources detected with AGILE in this work, according to the criteria described in the text.

ID	TeV source	$\sqrt{(TS)}$	(l, b) [deg]	Error (95%) ²⁰ [deg]	Flux ($E > 100$ MeV) [10^{-7} ph cm $^{-2}$ s $^{-1}$]	Dist. [deg]	AGILE association	Fermi association	Analysis flag
1	TeVJ0006+727	21.6	119.66, 10.51	0.09	3.3 ± 0.2	0.1	1AGLR J0007+7307	3FGL J0007.0+7302 (E)	IN
12	TeVJ0222+430	8.1	140.0, -16.7	0.2	1.4 ± 0.2	0.1	1AGLR J0222+4305	3FGL J0222.6+4301 (P)	IN
14	TeVJ0232+202	4.2	152.9, -36.3	0.6	1.1 ± 0.3	0.4	–	3FGL J0232.8+2016 (P)	IN
15	TeVJ0240+612	27.1	135.5, 1.2	0.1	6.6 ± 0.3	0.2	1AGLR J0240+6115	3FGL J0240.5+6113 (P)	E
19	TeVJ0319+415	5.5	150.6, -13.2	0.4	1.0 ± 0.2	0.1	1AGLR J0321+4137	3FGL J0319.8+4130 (P)	IN
24	TeVJ0521+211	4.7	183.6, -8.6	0.5	1.7 ± 0.4	0.1	–	3FGL J0521.7+2113 (P)	IN
26	TeVJ0534+220	55.9	184.48, -5.81	0.06	26.7 ± 0.7	0.1	1AGL J0535+2205	3FGL J0534.5+2201 (P)	IN
30	TeVJ0616+225	13.2	188.9, 3.0	0.2	5.0 ± 0.5	0.2	1AGL J0617+2236	3FGL J0617.2+2234e (E)	O
32	TeVJ0632+173	82.6	195.09, 4.28	0.04	41.8 ± 0.9	0.6	1AGL J0634+1748	3FGL J0633.9+1746 (E)	IN
36	TeVJ0721+713	13.9	143.9, 28.1	0.1	2.6 ± 0.2	0.1	1AGLR J0723+7121	3FGL J0721.9+7120 (P)	IN
45	TeVJ1018-589	7.8	284.0, -2.0	0.3	2.6 ± 0.4	0.3	1AGLR J1018-5852	{3FGL J1018.9-5856 (E) 3FGL J1016.3-5858 (E)}	O
49	TeVJ1104+382	5.2	179.7, 65.0	0.2	1.6 ± 0.4	0.1	1AGLR J1105+3818	3FGL J1104.4+3812 (P)	IN
60	TeVJ1256-057	11.2	305.3, 57.1	0.2	4.2 ± 0.5	0.1	1AGL J1256-0549	3FGL J1256.1-0547 (P)	IN
66	TeVJ1418-609	13.5	313.2, 0.1	0.1	5.1 ± 0.4	0.1	1AGLR J1417-6108	3FGL J1418.6-6058 (E)	IN
75	TeVJ1459-608	5.8	317.6, -1.7	0.3	1.6 ± 0.3	0.1	–	{3FGL J1456.7-6046 (E) 3FGL J1459.4-6053 (E)}	IN
79	TeVJ1512-091	25.0	351.4, 40.1	0.1	8.2 ± 0.4	0.1	1AGLR J1513-0906	3FGL J1512.8-0906 (P)	IN
87	TeVJ1632-478	5.7	336.4, 0.0	0.4	2.2 ± 0.4	0.2	–	3FGL J1633.0-4746e (E)	IN
88	TeVJ1634-472	15.2	337.4, 0.1	0.2	5.1 ± 0.5	0.3	1AGL J1639-4702	–	O
95	TeVJ1708-443	42.3	343.12, -2.69	0.06	13.9 ± 0.4	0.3	1AGL J1709-4428	3FGL J1709.7-4429 (E)	O
109	TeVJ1747-248	5.9	4.0, 1.7	0.3	2.1 ± 0.4	0.2	–	3FGL J1748.0-2447 (E)	O
112	TeVJ1801-233	15.0	6.6, 0.1	0.2	6.8 ± 0.5	0.4	1AGL J1801-2317	3FGL J1801.3-2326e (E)	E
113	TeVJ1804-216	7.8	8.4, 0.2	0.3	3.5 ± 0.5	0.2	1AGLR J1805-2149	3FGL J1805.6-2136e (E)	O
116	TeVJ1813-178	4.8	13.0, 0.4	0.4	2.1 ± 0.5	0.4	1AGL J1815-1732	–	IN
125	TeVJ1841-055	14.0	26.3, 0.1	0.2	5.8 ± 0.5	0.6	1AGLR J1839-0550	3FGL J1840.9-0532e (E)	O
128	TeVJ1848-017	4.6	30.8, 0.1	0.2	1.8 ± 0.4	0.4	–	3FGL J1848.4-0141 (E)	O
132	TeVJ1907+062	13.3	40.4, -1.0	0.1	4.4 ± 0.4	0.2	1AGL J1908+0614	3FGL J1907.9+0602 (E)	O
133	TeVJ1911+090	7.8	43.3, 0.0	0.3	2.4 ± 0.3	0.2	–	–	IN
135	TeVJ1923+141	7.1	49.2, -0.5	0.3	2.1 ± 0.3	0.2	1AGL J1923+1404	3FGL J1923.2+1408e (E)	IN
142	TeVJ2019+368	25.5	75.17, 0.25	0.09	6.9 ± 0.3	0.2	1AGLR J2021+3653	3FGL J2021.1+3651 (E)	IN
144	TeVJ2032+415	8.0	80.3, 1.2	0.2	2.3 ± 0.3	0.1	1AGLR J2031+4130	3FGL J2032.2+4126 (E)	O
145	TeVJ2158-302	4.8	17.6, -52.0	0.6	1.4 ± 0.3	0.3	–	3FGL J2158.8-3013 (P)	IN
147	TeVJ2227+608	16.7	106.7, 3.0	0.2	3.3 ± 0.2	0.4	1AGL J2231+6109	3FGL J2225.8+6045 (E)	E
152	TeVJ2359-306	4.0	12.6, -78.0	0.3	3.3 ± 1.0	0.1	–	3FGL J2359.3-3038 (P)	IN

Notes. The upper part reports the results of the MLE analysis, Step 3, and the lower part the results of Step 4. ⁽²⁰⁾ The AGILE team recommends adding a systematic error of $\pm 0.1^\circ$ linearly.

Table A.2. continued.

ID	TeV source	$\sqrt{(TS)}$	(<i>l</i> , <i>b</i>) [deg]	Error (95%) ²⁰ [deg]	Flux (<i>E</i> > 100 MeV) [10 ⁻⁷ ph cm ⁻² s ⁻¹]	Dist. [deg]	AGILE association	Fermi association	Analysis flag
38	TeVJ0835-455 ¹²	7.9	-, -	-	6.2 ± 0.8	-	-	3FGL J0833.1-4511e (E)	-
40	TeVJ0852-463 ¹³	4.0	-, -	-	1.5 ± 0.4	-	-	3FGL J0852.7-4631e (E)	-
64	TeVJ1325-430 ¹⁶	4.4	-, -	-	0.8 ± 0.2	-	-	3FGL J1325.4-4301 (P)	-
89	TeVJ1640-465	12.3	-, -	-	5.1 ± 0.5	-	1AGL J1639-4702	3FGL J1640.4-4634c (E)	-
96	TeVJ1713-382	6.5	-, -	-	2.6 ± 0.4	-	-	-	-
98	TeVJ1714-385 ¹⁸	7.0	-, -	-	2.8 ± 0.4	-	-	3FGL J1714.5-3832 (E)	-
99	TeVJ1718-374	6.2	-, -	-	2.6 ± 0.4	-	-	3FGL J1718.0-3726 (P)	-
100	TeVJ1718-385	6.9	-, -	-	2.7 ± 0.4	-	-	3FGL J1718.1-3825 (E)	-
103	TeVJ1729-345	8.0	-, -	-	3.6 ± 0.5	-	-	-	-
104	TeVJ1732-347	7.3	-, -	-	3.1 ± 0.5	-	-	-	-
105	TeVJ1741-302 ¹⁹	4.3	-, -	-	2.1 ± 0.5	-	-	-	-
108	TeVJ1745-303	11.2	-, -	-	5.5 ± 0.5	-	1AGL J1746-3017	3FGL J1745.1-3011 (E)	-
118	TeVJ1825-137	8.0	-, -	-	3.8 ± 0.5	-	-	3FGL J1824.5-1351e (E)	-
119	TeVJ1826-148 ¹⁸	7.7	-, -	-	3.3 ± 0.5	-	-	3FGL J1826.2-1450 (P)	-
124	TeVJ1837-069	4.9	-, -	-	2.1 ± 0.4	-	-	3FGL J1836.5-0655e (E)	-
134	TeVJ1912+101	4.1	-, -	-	1.3 ± 0.3	-	-	-	-
139	TeVJ2001+438	4.9	-, -	-	0.9 ± 0.2	-	-	3FGL J2001.1+4352 (P)	-
146	TeVJ2202+422	7.2	-, -	-	1.0 ± 0.2	-	-	3FGL J2202.7+4217 (P)	-
150	TeVJ2323+588	5.2	-, -	-	0.9 ± 0.2	-	-	3FGL J2323.4+5849 (P)	-

Table A.3. Results of the spectral analysis of the most significant sources detected with AGILE in this analysis.

ID	TeV Source	Type	AGILE power-law spectral index ²¹	AGILE association	Fermi association	3FGL power-law spectral index ²²
1	TeVJ0006+727	PWN	1.91 ± 0.05	1AGLR J0007+7307	3FGL J0007.0+7302	1.88
12	TeVJ0222+430	IBL	2.04 ± 0.10	1AGLR J0222+4305	3FGL J0222.6+4301	1.94
15	TeVJ0240+612	XRB	2.19 ± 0.04	1AGLR J0240+6115	3FGL J0240.5+6113	2.29
19	TeVJ0319+415	FRI	1.80 ± 0.14	1AGLR J0321+4137	3FGL J0319.8+4130	2.08
26	TeVJ0534+220	PWN	2.27 ± 0.03	1AGL J0535+2205	3FGL J0534.5+2201	2.23
30	TeVJ0616+225	SNR	1.95 ± 0.07	1AGL J0617+2236	3FGL J0617.2+2234e	1.98
32	TeVJ0632+173	PWN	1.88 ± 0.02	1AGL J0634+1748	3FGL J0633.9+1746	1.87
36	TeVJ0721+713	LBL	1.87 ± 0.07	1AGLR J0723+7121	3FGL J0721.9+7120	2.04
45	TeVJ1018-589	BIN	2.07 ± 0.11	1AGLR J1018-5852	{3FGL J1016.3-5858 3FGL J1018.9-5856	{2.35 2.30
66	TeVJ1418-609	PWN	2.00 ± 0.07	1AGLR J1417-6108	3FGL J1418.6-6058	2.27
75	TeVJ1459-608	PWN	2.16 ± 0.12	–	{3FGL J1456.7-6046 3FGL J1459.4-6053	{2.37 2.37
87	TeVJ1632-478	UNID	2.05 ± 0.14	–	3FGL J1633.0-4746e	2.11 ± 0.02
88	TeVJ1634-472	UNID	2.58 ± 0.08	1AGL J1639-4702	–	–
95	TeVJ1708-443	PWN	2.02 ± 0.02	1AGL J1709-4428	3FGL J1709.7-4429	2.02
109	TeVJ1747-248	GC	1.99 ± 0.17	–	3FGL J1748.0-2447	2.26
112	TeVJ1801-233	SNR/MC	2.07 ± 0.07	1AGL J1801-2317	3FGL J1801.3-2326e	2.15
113	TeVJ1804-216	UNID	2.13 ± 0.12	1AGLR J1805-2149	3FGL J1805.6-2136e	2.07
125	TeVJ1841-055	UNID	2.41 ± 0.08	1AGLR J1839-0550	3FGL J1840.9-0532e	1.81 ± 0.04
132	TeVJ1907+062	UNID	2.36 ± 0.07	1AGL J1908+0614	3FGL J1907.9+0602	2.24
133	TeVJ1911+090	SNR/MC	2.21 ± 0.12	–	–	–
135	TeVJ1923+141	SNR/MC	2.23 ± 0.12	1AGL J1923+1404	3FGL J1923.2+1408e	2.15
142	TeVJ2019+368	PWN	1.98 ± 0.04	1AGLR J2021+3653	3FGL J2021.1+3651	2.17
144	TeVJ2032+415	UNID	2.05 ± 0.10	1AGLR J2031+4130	3FGL J2032.2+4126	2.08
147	TeVJ2227+608	SNR	2.30 ± 0.06	1AGL J2231+6109	3FGL J2225.8+6045	1.95 ± 0.20

Notes. The spectral indexes for all sources that were detected with a significance $\sqrt{(TS)}_3 > 5$ (see upper part of Table A.2) and Galactic latitude $|b| < 30^\circ$ are reported. The last column shows the Fermi *power-law index* as given in the indicated reference; when the Fermi sources spectrum has been fitted with a power-law function (i.e. the spectral form is PowerLaw), the corresponding error is also available and reported. ⁽²¹⁾ This analysis. ⁽²²⁾ (Acero et al. 2015). The errors on the Fermi power-law spectral indices in the 3FGL catalog are available only for three sources: 3FGL J1633.0-4746e, 3FGL J1840.9-0532e, 3FGL J2225.8+6045. See also footnote⁽⁵⁾.

Table A.4. Statistics about the sources detected by AGILE in this work, grouped by source type classification.

Source type	Detected/Total	Source class	Detected/Total
Extragalactic	13/66 (20%)	Blazar	0/1 (0%)
		HBL	5/44 (11%)
		IBL	2/7 (29%)
		LBL	2/3 (67%)
		FSRQ	2/5 (40%)
		Sbs	0/2 (0%)
		Superbubble	0/1 (0%)
Galactic	30/58 (52%)	FRI	2/3 (67%)
		PWN	11/28 (39%)
		SNR	7/11 (64%)
		PWN/SNR	2/2 (100%)
		SNR/MC	5/8 (63%)
		BIN/XRB	3/5 (60%)
		GC	1/1 (100%)
Unidentified	9/28 (32%)	WR	1/3 (33%)
		–	–

Notes. Enclosed in parenthesis, the percentage of detected sources with respect to the total class sample.